Simulating the microstructural evolution of a Selective Laser Melted AA-2024

Omar López[1], Uriel Martínez-Hernández[2], José Ramírez[3], Christophe Pinna[1], Kamran Mumtaz[1]

[1] Department of Mechanical Engineering, University of Sheffield, Sheffield, UK.
[2] Department of Automatic Control and Systems Engineering, University of Sheffield, Sheffield, UK.
[3] Centro de Investigación e Innovación en Ingeniería Aeronáutica, Facultad de Ingeniería Mecánica y Eléctrica, Universidad Autónoma de Nuevo León, Monterrey, Nuevo León, México.

Abstract

A two-dimensional Cellular Automata (CA) – Finite Element (FE) (CA-FE) coupled model has been developed in order to predict the microstructure formed during melting of a powdered AA-2024 feedstock using the Additive Manufacturing (AM) process Selective Laser Melting (SLM). The presented CA model is coupled with a detailed thermal FE model computing heat flow characteristics of the SLM process. The developed model takes into account the powder-to-liquid-to-solid transformation, tracks the interaction between several melt pools within a melted track, and several tracks within various layers. It was found that the simulated microstructures bared a close resemblance with fabricated AA-2024 SLM samples. With these observed capabilities of the model, the porosity within a SLM produced part can be predicted, and used to optimise the fabrication parameters of a sample.

Introduction

The SLM process is an AM technology generally used for the manufacture of complex high value products (i.e. within aerospace, automotive sectors). The geometric freedom, short component development lead times and as-built material performance gives this technology distinct advantages over conventional manufacturing techniques. Numerical methods that simulate the SLM process have been undertaken by several researchers. Each of these numerical approaches attempts to develop an improved understanding of the physical phenomena that occur during the laser processing of a powder bed (thermal history, Marangoni flows, solidification front, etc.).

The thermal history generated to a component manufactured via SLM has been a main area of investigation. Shiomi et al. [1] proposed an FE simulation that calculated the temperature distribution within metallic powders exposed to a pulsed laser and found that the maximum temperature reached by the metallic powder was affected by the peak laser power rather than the duration of the laser irradiation. Matsumoto et al. [2] was one of the first researchers to compute the change from powder-to-liquid-to-solid and proposed a method to calculate the temperature and stress distribution within a solidified layer within the SLM process using the FE method. Roberts et al. [3] developed a three-dimensional model in order to understand the thermal history resulting from the layer-by-layer processing. Even though their results agree with experiments, a more detailed model is needed in order to compute the solidification phenomena within SLM. Loh et al. [4] developed a single layer FEM model that uses a sacrificial layer (which vaporises) in order to obtain accurate results, however this approach is not suitable for a multilayer process. Foroozmehr et al. [5] used the optical penetration depth of a laser beam [6] and developed a 3D single layer

powder bed model to predict the temperature profiles. The obtained results are considered accurate, however, the model does not consider the interaction between layers. In an attempt to predict optimal processing parameters during SLM, Song et al. [7] simulated the process on a three-dimensional FE model and then experimentally validated the results, highlighting the importance of a FEM simulation of the SLM process. It has been shown that numerical models of the SLM process are important in order to achieve a certain degree of control/optimisation of the process [8].

Heat transfer within a melt pool formed by the SLM process is highly influenced by the fluid flow [9] present in the melt, solely modelling laser melting process without fluid flow will cause inaccuracies. Khairallah et al. [10] demonstrated via a three-dimensional mesoscopic micrometre scale model the importance of including the stochastic nature of the powder bed. It was found that the physics of the process is driven by the surface tension of the melt pool and subsequently effects the heat transfer and topology of the solidified melt pools. Pengpeng et al. [11] used Computational Fluid Dynamics (CFD) to accurately predict the melt pool geometry and temperature distributions present within the process. Through the use of CFD models there is the capability to accurately predict melt pool geometries (depth, width, overlap, etc.) and thermal distributions. These require a certain degree of expertise of fluid dynamics and longer computational time as compared to FE heat transfer models. The enhanced thermal conductivity approach has been used in order to simplify and reduce the simulation processing time. Safdar et al. [8] state that the enhanced thermal conductivity approach is able to artificially simulate the melt pool convection during the processing of materials in SLM without the need of CFD models.

SLM microstructural studies have mainly focussed in observations of experimentally fabricated components. Yin and Felicelli [12] developed a numerical model of the microstructural development present in the Laser Engineering Net Shaping (LENS) process focussing on a micro region of the melt pool. The developed model does not consider convection on the top surface of the layer, and the obtained results are only relevant for the deposition of a single layer according to the researchers.

Different numerical simulations are available and used to understand grain growth and develop optimum processing conditions in other metal processing techniques (i.e. casting, forging, etc.). Despite the benefits that numerical simulations offer, the development of an appropriate numerical simulation to model microstructural evolution within powder bed SLM has not yet been reported in literature. This research develops a “first of its kind” microstructural evolution model of the SLM process. The model is based on the CA-FE method developed by Gandin and Rappaz [13]. The CA-FE technique is used in order to develop a new model which is able to capture the evolution of the microstructural formation during the melting-solidification of various melt pools within several layers of the SLM process.

Thermal History Model

Laser Governing Equations

A localised laser beam is used in SLM in order to melt the powder bed. The present work models the heat source using a Gaussian model. The approximation of the heat source used by Shi et al. (2007), expressed as:

$$\ddot{\phi} = 0.864\alpha \frac{P}{\pi r^2}$$

where P is the power of the laser beam, α is the laser energy absorptance of the material and r is the spot radius is used in the present research.

The corresponding calculations on the time-dependent temperature distribution during the SLM process were performed with the FE software ANSYS Ver. 14.0.

Temperature dependent material properties

In the current work the material investigated is AA-2024, due to its associated use and interest in industries such as aerospace. The temperature dependent properties of the powdered AA-2024 material within this work substitutes the discrete powder bed by a continuum material that possess equivalent material properties in order to compute the effective material properties of the powder bed as that proposed by Sih and Barlow [14]. The density of the powder at room temperature was experimentally obtained by measuring the mass of a container of a known volume filled with powder and temperature dependent values established by considering the expected behaviour of the powder when heated.

The thermophysical properties of the liquid phase differ from those of the solid alloy (e.g. thermal conductivity and density) thus the value of the thermophysical property in the mushy region will be dependent on the amount of liquid and solid (i.e. solid fraction). In order to calculate the required property (P) at a certain temperature (T), the expression proposed by Mills [15] is used:

$$P_T = f_{s(T)} P_{T_{sol}} + \left(1 - f_{s(t)}\right) P_{T_{liq}}$$

where $f_{s(T)}$ is the solid fraction at a defined temperature, P_{Tsol} and P_{Tliq} are the values of the property of interest at the solidus and liquidus temperature respectively. This expression is used in this research to compute the density, heat capacity, enthalpy of fusion, thermal conductivity, diffusivity and emissivity in the mushy region of a material.

In order to mimic the fluid flow present in a melt pool generated during the SLM process, the enhanced thermal conductivity approach is used, where the thermal conductivity λ''_{ii} is defined as:

$$\lambda''_{ii} = \alpha''_{ii} k$$

where k is the normal isotropic thermal conductivity value at the corresponding temperature, ii represent the spatial coordinate and α''_{ii} is the anisotropic enhancement factor for the respective spatial coordinate, which is defined as:

$$\alpha''_{ii} = \begin{cases} 1 & if\ T < T_{liquidus}\ \&\ T_{solidus} \\ Multiplying\ factor & if\ T > T_{liquidus} \end{cases}$$

In the developed simulation several enhancement factors were used depending on the laser power employed during processing and will be enlisted on Table 1. The material data used for the FEM are shown in Figure 1.

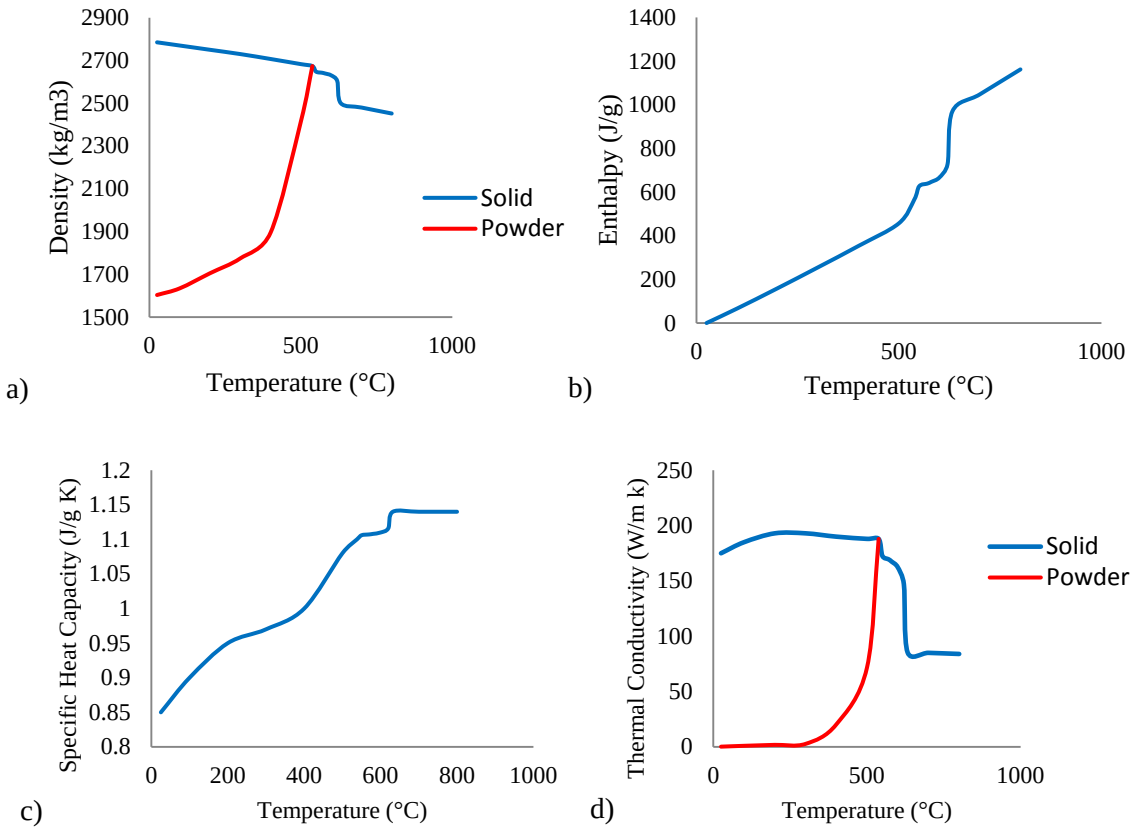

Figure 1. Thermal dependent a) density, b) enthalpy, c) specific heat and d) thermal conductivity.

Simulation model description

A two-dimensional rectangular model was meshed with rectangular elements. 2D thermal conduction solid elements (SOLID77) with 8 nodes and a single degree of freedom, temperature, at each node were used. The model is constructed with four 50µm high layers of AA-2024 in the form of powder and a block of 0.5mm of height and 2mm of width of solid form AA-2024. In order to simulate the heat dissipation along the powder bed (without interfering with the temperature distribution generated by the laser heat source in the scanned region), temperature boundary conditions were defined (applied to all the walls of the model).

The developed model reproduces the layer-by-layer building methodology employed by SLM. Within the calculations, the chamber temperature is maintained at 80°C. The laser (with diameter of 50μm) is applied as a heat flux on the powder bed surface at the corresponding location for a defined time (dictated by the exposure time). The layers are then deposited in the model using the element birth and death technique. After the irradiation time of a layer has finished, a recoating time (12s) is simulated. This routine is continued layer-by-layer until the last layer is complete.

Cellular Automata model

The nucleation and growth kinetics involved during the solidification process are calculated within the CA model. The developed model mimics the development of grain structures by changing the state indices of the cells in the CA grid. The nucleation and the growth kinetics are temperature dependent so the temperature values are determined by the FE model developed. The cells (v) of the CA grid are first initialised with values of the state index corresponding to the values indicated by the initial time step of the FE nodes. When the local temperature of a cell (ΔT_v^t) becomes lower than the critical temperature for the nucleation site (ΔT^{nucl}), a new grain is created. The nucleation undercooling temperatures follow a Gaussian distribution [16]. Subsequently a unique grain number is attributed to the cell (v) for each nucleation event and its state index is updated corresponding to a non-liquid state.

In the case of the growth algorithm, the growth only occurs if the local temperature corresponds to the defined growth undercooling temperature. The index state of the neighbouring cell is then switched to a value that corresponds to the growing grain structure. If a liquid cell is captured by several neighbouring cells during the same time step, a randomly selected neighbouring cell will capture that liquid cell and transform it into solid.

Cellular Automata – coupling with Finite Element

The local temperature or undercooling temperatures of the cells are calculated through FE and are a key parameter of the CA nucleation-growth algorithm. The CA-FE method superimposes the FE mesh to the CA lattice. A weak or a full coupling mode can be used [17]. In this research the weak coupling mode was used, in which a unique solidification path (e.g. the Gulliver-Sheil micro-segregation path) is used on the FE calculation. The variation of enthalpy is then a simple function of temperature variation alone and the temperature field is directly solved on the macroscopic scale. The CA rules defined uses the values of temperature distributions calculated by the FE at certain time intervals.

Results and discussion

Thermal History Simulation Validation

To determine the suitability of the developed model, experimental work was conducted. Several experiments were undertaken, varying processing parameters (as shown in Table 1) in both the simulation and the experimental trials. Consequently, the melt pool size (height and diameter) of the benchmark samples was measured and compared to that of the obtained simulation in order to calibrate the model. SLM samples were then created to validate the results of the numerical simulation.

Table 1. SLM processing parameters.

Sample	*Power (W)*	*Point Distance (μm)*	*Exposure time (μs)*	α_{xx}	α_{yy}
1	200	25	450	3.0	1.5
2	200	35	450	3.0	1.5
3	180	30	350	15.0	8.0
4	170	60	400	25.0	15.0
5	170	60	300	25.0	15.0
6	170	50	300	25.0	15.0
7	170	50	400	25.0	15.0

The samples used for metallographic inspection were grinded and polished according to standard procedures and etched using Keller's reagent (solution consisting of 190 ml distilled water, 5 ml HNO_3, 3ml HCl, 2 ml HF). Melt pools were measured in different locations of the sample and an average size of melt pool was determined per specimen. Approximately 3 to 5 measurements were performed to ten micrographs obtained per sample.

In Table 2 the obtained data of both the experimental and the simulated data for melt pool geometry is shown. The presented data suggests that a 14% error is present between the experimental and modelling results, thus the prediction of the melt pool dimensions of parts produced in the SLM system can be performed within this limit.

Table 2. Measured Melt Pool Size

Sample	*Experimental mean diameter (μm)*	*Standard deviation of measured diameter*	*Experimental mean depth (μm)*	*Standard deviation of measured depth*	*Maximum Predicted Diameter (μm)*	*Maximum Predicted Depth (μm)*
1	237.82	38.71	77.6	11.58	235	75
2	205.77	19.58	74.66	8.84	220	75
3	205.46	37.98	76.05	11.69	195	65
4	202.41	24.97	82.09	13.23	210	75
5	200.14	22.3	78.58	11.94	195	70
6	179.22	20.60	73.99	8.80	205	70
7	208.56	26.10	82.7	11.15	210	75

Thermal History Analysis

From the developed 2D layer-by-layer FEM model, valuable data can be extracted. Information such as cooling and solidification rates of the melt pool and porosity can be used. Cooling rates for Rapid Solidification Processes (RSP) are in the range of 10^5 to 10^6K/s [18]. Kurz and Trivedi outlined the solidification conditions of a process similar to SLM, laser surface processing; a relationship between the cooling rate ($|\dot{T}|$), the thermal gradient in the liquid ahead of the solid-liquid interface (G) and the interface growth rate (V) was established, which is defined as $|\dot{T}| = G * V$. It was determined that the solidification conditions of that of laser processing will in most the cases, lead to a columnar (directional) growth [19]. In Table 3 the cooling rate, the thermal gradient in the liquid, the solidification rate and the calculated mean V are shown.

Table 3. Mean cooling and solidification rates extracted from the developed FEM for each simulated sample.

Sample Number	*Mean cooling rate of the liquid (K/s)*	*Mean solidification rate (K/m)*	*Thermal gradient in the liquid (K/m)*	*Calculated mean V (m/s)*
1	4.3×10^5	2.66×10^6	3.5×10^6	0.12
2	5.41×10^5	2.14×10^6	2.9×10^6	0.18
3	1.12×10^5	1.91×10^6	1.7×10^6	0.07
4	1.55×10^5	1.67×10^6	1.7×10^6	0.09
5	2.11×10^5	1.35×10^6	2.2×10^6	0.1
6	1.45×10^5	1.35×10^6	2.2×10^6	0.07
7	1.15×10^5	1.82×10^6	2.0×10^6	0.06

The data obtained from the developed FEM model suggests that the resulting microstructure of the sample will be dendritic. Simulated results also agree with calculated values of cooling rates determined by Harrison et al. [20], determined using measurements of primary dendrite arm spacing of parts produced with SLM. Following the inverse procedure used by Harrison et al., the primary dendrite arm spacing on parts produced by SLM could also be predicted.

When a new material is to be manufactured in SLM a full Design of Experiments (DOE) is undertaken in order to find the optimal processing parameters. The DOE process and stages leading up to parameter optimisation can be more efficient if aided by the FEM model developed in this work. The developed FEM model predicts the 2D porosity generated for a set of SLM parameters known to produce porous components, as shown in Figure 2.

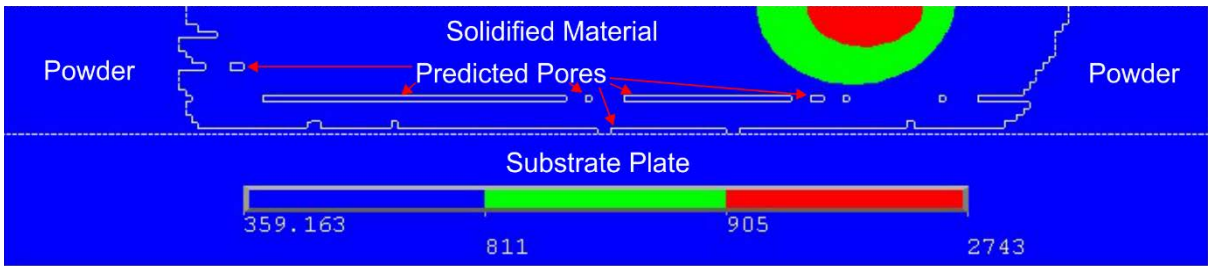

Figure 2 - Predicted porosity on developed FEM model of sample number 7.

The dashed line in Figure 2 delimits the substrate plate from the powder bed, the solid line envelopes the formed solid after the irradiation of the laser beam. A certain level of porosity is observed in the calculated results by the FEM model, and it can be said that the model can predict (with limitations) when a layer will not be fully melted and when porosity will be generated due to the lack of melting.

Microstructural evolution, simulation and validation

A similar validation process to that used to validate the thermal history is used to determine the suitability of the developed microstructural evolution model. Using the set of parameters shown in Table 1, benchmark specimens were produced and results were inputted into the

simulation for calibration, validation SLM samples were then fabricated and the microstructure was compared with the simulation results.

The samples were grinded and polished according to standard procedures and anodized with Baker's reagent (solution of 1.8% HBF_4 in water, using 20 Vdc for 80s and an agitation velocity of 10RPM at 22°C). The Average Grain Size Number (AGSN) was measured in different locations of the specimens along the transverse direction of the elongated grains in order to determine an average grain size number per specimen according to the procedures mentioned in ASTM E112 standards. Measurements along the length direction of the grains were not performed, since the numerical model is only representative for four layers and the experimental values will be representative for the whole sample size. The orientation of the grains as well as the development of a grain within layers was observed and visually compared with the obtained simulated results. An average of 50 measurements per sample were performed in order to determine the AGSN. The calculations performed by the developed CA-FE model were exported into a .bmp file in order to have a visual comparison with experimental data, different colours (red, green, blue and pink) will determine different grains.

Table 4 shows the data of both the experimental and predicted AGSN. The shown data suggests that a 12% error between measurements and predictions is present.

Table 4. Experimental and Predicted Average Grain Size Number

Sample	Experimental AGSN	StdDev	Predicted AGSN	StdDev
1	8.32	0.46	8.47	0.59
2	8.47	0.65	8.07	1.62
3	9.05	0.40	9.34	0.60
4	8.11	0.34	9.31	0.67
5	9.05	0.48	9.13	0.23
6	8.71	0.59	9.13	0.39
7	8.66	0.51	9.42	0.83

Microstructural analysis results of the multilayer model.

The developed CA model along the calculated temperature profiles by the developed FEM model (CA-FE) is able to predict the microstructural evolution of a part produced by SLM. The developed CA-FE model requires of data obtained from fabricated benchmark samples, in order to successfully predict the microstructure. The required data (the probability of nucleation) is then inputted to the developed code. The probability of nucleation depends of the material to be used, in the case of the present work this probability was established as 0.025 based on experimental observations and trial and error runs of the code.

The predicted AGSN agrees with experimental information data with a 12% error. In addition, making a close comparison of the predicted microstructure with the microstructure obtained from experiments (see Figure 3), columnar grains that grow between layers with smaller equiaxed type interspersed grains can be observed in both microstructures. Grain boundaries intersecting primary columnar grains are occasionally formed at the limits of each melt pool within the prediction (as

observed in Figure 3a & 3c), comparable to the observed phenomenon in the experiments (as observed in Figure 3b & 3d), as well as in the research undertaken by Harrison et al. [20]. New formed grains continue to grow and competitive growth has then an important role in the layer-by-layer process.

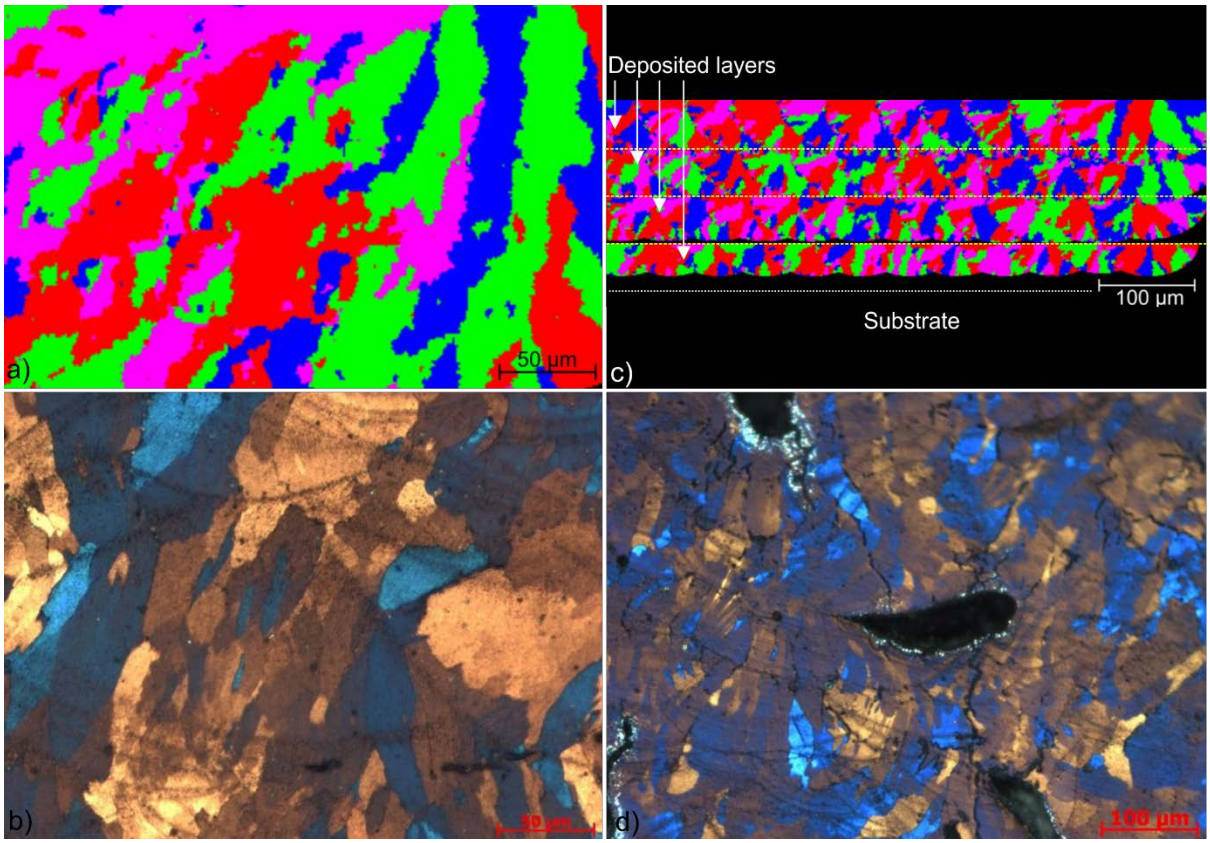

Figure 3 - a) Predicted microstructure vs b) actual microstructure of sample with almost null pores present (sample 1), and c) predicted microstructure vs d) actual microstructure of sample with pores present (sample 6).

Conclusions

A 2D FEM layer-by-layer model that considers the most important processing parameters in SLM (e.g. laser power, point distance, exposure time, etc.) as well as detailed material properties (e.g. absorptance, density, thermal conductivity, etc.) was developed. The developed 2D FEM model successfully predicts the generated thermal history within the SLM process.

A CA model that imports the temperature profiles calculated by the developed 2D FEM model was developed (CA-FE) in order to predict the solidification phenomenon present within the SLM process. The CA-FE model is able to predict the microstructures formed in components manufactured via SLM.

A first set of samples were produced to validate both FEM and CA-FE models. The melt pool size and the AGSN were measured in order to calibrate the developed models. A second set of samples was measured and the obtained results were then compared with the predicted results. The

developed 2D FEM model predicted the melt pool dimensions with an error of approximately 14%, and the developed CA-FE model predicted the AGSN with an error of approximately 12%. With this values it is concluded that both models successfully predict both the temperature profiles and the microstructures of components manufactured via SLM.

Useful data was extracted from the developed models. The cooling and solidification rates were calculated, and it was confirmed that the process can be considered as a RSP technique. Using the GV microstructure selection map [19], it was determined that the formed microstructure would be composed of dendritic growth. Porosity, was predicted by the developed FEM model as a result of lack of fusion. These predictions are useful in order to avoid such defects by running multiple simulations in order to minimise porosity. As future work, further validations on porosity predictions is required in order to fully rely on the results obtained from the FEM model.

The predicted microstructures by the developed CA-FE model are similar to those of components manufactured via SLM. They both present similar growth phenomena as well as the formation of small equiaxed grains at the liquid interface of the formed melt pools, which then will compete with larger columnar grains and grow towards the general heat flux. This results in the appearance of small dispersed grains and columnar grains that halted growth between layers due to these dispersed grains. It is concluded that the predicted microstructure agrees with experiments.

Acknowledgements

The authors would like to thank the EPSRC Centre for Innovative Manufacturing – Liquid Metal Engineering (grant number EP/H026177/1) and the National Council of Science and Technology of Mexico (CONACyT) for support during this project.

References

[1] M. Shiomi, A. Yoshidome, F. Abe, K. Osakada. Finite element analysis of melting and solidifying processes in laser rapid prototyping of metallic powders, International Journal of Machine Tools and Manufacture 39 (1999) 237-252.
[2] M. Matsumoto, M. Shiomi, K. Osakada, F. Abe. Finite element analysis of single layer forming on metallic powder bed in rapid prototyping by selective laser processing, International Journal of Machine Tools and Manufacture 42 (2002) 61-67.
[3] I.A. Roberts, C.J. Wang, R. Esterlein, M. Stanford, D.J. Mynors. A three-dimensional finite element analysis of the temperature field during laser melting of metal powders in additive layer manufacturing, International Journal of Machine Tools and Manufacture 49 (2009) 916-923.
[4] L.-E. Loh, C.-K. Chua, W.-Y. Yeong, J. Song, M. Mapar, S.-L. Sing, Z.-H. Liu, D.-Q. Zhang. Numerical investigation and an effective modelling on the Selective Laser Melting (SLM) process with aluminium alloy 6061, International Journal of Heat and Mass Transfer 80 (2015) 288-300.
[5] A. Foroozmehr, M. Badrossamay, E. Foroozmehr, S.i. Golabi. Finite Element Simulation of Selective Laser Melting process considering Optical Penetration Depth of laser in powder bed, Materials & Design 89 (2016) 255-263.

[6] P. Fischer, N. Karapatis, V. Romano, R. Glardon, H.P. Weber. A model for the interaction of near-infrared laser pulses with metal powders in selective laser sintering, Appl Phys A 74 (2002) 467-474.
[7] B. Song, S. Dong, H. Liao, C. Coddet. Process parameter selection for selective laser melting of Ti6Al4V based on temperature distribution simulation and experimental sintering, The International Journal of Advanced Manufacturing Technology 61 (2012) 967-974.
[8] S. Safdar, A.J. Pinkerton, L. Li, M.A. Sheikh, P.J. Withers. An anisotropic enhanced thermal conductivity approach for modelling laser melt pools for Ni-base super alloys, Applied Mathematical Modelling 37 (2013) 1187-1195.
[9] K.C. Mills, B.J. Keene, R.F. Brooks, A. Shirali. Marangoni effects in welding, Philosophical Transactions of the Royal Society of London A: Mathematical, Physical and Engineering Sciences 356 (1998) 911-925.
[10] S.A. Khairallah, A. Anderson. Mesoscopic simulation model of selective laser melting of stainless steel powder, Journal of Materials Processing Technology 214 (2014) 2627-2636.
[11] Y. Pengpeng, G. Dongdong. Molten pool behaviour and its physical mechanism during selective laser melting of TiC/AlSi10Mg nanocomposites: simulation and experiments, Journal of Physics D: Applied Physics 48 (2015) 035303.
[12] H. Yin, S.D. Felicelli. Dendrite growth simulation during solidification in the LENS process, Acta Materialia 58 (2010) 1455-1465.
[13] C.-A. Gandin, M. Rappaz. A Coupled Finite Element - Cellular Automaton Model for the Prediction of Dendritic Grain Structures in Solidification Processes, Acta Materialia 42 (1994) 2233-2246.
[14] S. Sumin Sih, J.W. Barlow. The Prediction of the Emissivity and Thermal Conductivity of Powder Beds, Particulate Science and Technology 22 (2004) 291-304.
[15] K.C. Mills. Recommended Values of Thermophysical Properties for Selected Commercial Alloys, Woodhead Publishing Limited, 2002.
[16] M. Rappaz. Modelling of microstructure formation in solidification processes, International Materials Reviews 34 (1989) 93-124.
[17] C.-A. Gandin, J.L. Desbiolles, M. Rappaz, P. Thevoz. A Three-Dimensional Cellular Automaton - Finite Element Model for the Prediction of Solidification Grain Structures, Metallurgical and Materials Transactions A 30A (1999) 3153-3165.
[18] L.A. Jacobson, J. McKittrick. Rapid solidification processing, Materials Science and Engineering: R: Reports 11 (1994) 355-408.
[19] W. Kurz, R. Trivedi. Proceedings of the Eighth International Conference on Rapidly Quenched and Metastable Materials Rapid solidification processing and microstructure formation, Materials Science and Engineering: A 179 (1994) 46-51.
[20] N.J. Harrison, I. Todd, K. Mumtaz. Reduction of micro-cracking in nickel superalloys processed by Selective Laser Melting: A fundamental alloy design approach, Acta Materialia 94 (2015) 59-68.